International Journal of Heat and Mass Transfer 53 (2010) 1164–1174

Contents lists available at ScienceDirect

International Journal of Heat and Mass Transfer

journal homepage: www.elsevier.com/locate/ijhmt

Enhancing heat transfer in the core flow by using porous medium insert in a tube

Z.F. Huang [a], A. Nakayama [b], K. Yang [a], C. Yang [a,b], W. Liu [a,*]

[a] School of Energy and Power Engineering, Huazhong University of Science and Technology, Wuhan 430074, China
[b] Department of Mechanical Engineering, Shizuoka University, 3-5-1 Johoku, Hamamatsu 432-8561, Japan

ARTICLE INFO

Article history:
Received 24 February 2009
Received in revised form 23 September 2009
Accepted 7 October 2009
Available online 11 December 2009

Keywords:
Heat transfer enhancement
Porous media
Core flow
Tube

ABSTRACT

According to the concept of heat transfer enhancement in the core flow, porous media with a slightly smaller diameter to a tube are developed and inserted in the core of the tube under the constant and uniform heat flux condition. The flow resistance and heat transfer characteristics of the air flow for laminar to fully turbulent ranges of Reynolds numbers are investigated experimentally and numerically. There are three different porous media used in the experiments with porosity of 0.951, 0.966 and 0.975, respectively. The effect of porous radius ratio on the heat transfer performance is studied in numerical simulation. Both numerical and experimental results show that the convective heat transfer is considerably enhanced by the porous inserts of an approximate diameter with the tube and the corresponding flow resistance increases in a reasonable extent especially in laminar flow. It shows that the core flow enhancement is an efficacious method for enhancing heat transfer.

1. Introduction

In the development of modern industrial world, tremendous works on heat transfer enhancement have been conducted and a large number of techniques for convective heat transfer enhancement have been developed since 1970s. Most of these techniques are targeted at the tube fluid flow. The flow in a pipe can be divided into two parts [1]: boundary flow, which represents boundary layer in the entrance length or the fluid layer near wall in the fully developed length, and core flow. To raise the heat transfer efficiency of heat exchangers, most attentions have been paid to the surface of tube [2]. The commonly used methods are: (a) disrupting the fluid boundary layer near the wall; (b) extending the solid surface to transfer more heat flux; (c) changing the physical and chemical natures of the surface, etc. This kind of methods is focused on the heat transfer boundary and thus it may be called heat transfer enhancement in the boundary flow. However, when these methods effectively increase the amount of heat transferred, they also increase the flow resistance inevitably: as the velocity gradient, viscous diffusion as well as the momentum loss of the fluid near the boundary increases, the shearing strength and friction between the fluid and boundary may have different extents of growth.

Different from traditional manner of heat transfer enhancement, Liu et al. [3] developed the new concept of enhanced heat transfer in the core flow along a tube. He believes that the core flow of tubes is worthy to be well used for heat transfer augmentation. The most direct way is to make temperature as uniform as possible in the core flow of the tube in order to form a thin thermal boundary layer near the wall with great temperature gradient, thus resulting in a significant heat transfer enhancement effect. At the same time, it is necessary to: (a) minimize the velocity gradient of the tube flow for avoiding excessive fluid shear stress; (b) keep hydrodynamic boundary apart from disturbance for preventing redundant loss of fluid momentum; and (c) interrupt the continuously extended surfaces to be discontinuous as far as possible to decrease surface frictional resistance. So, the essentials of the method can be mainly summarized as: (a) making temperature uniform in the core flow; (b) not to increase velocity gradient in the flow field; (c) not to disrupt fluid near the boundary; (d) not to extend continuous surface on the wall.

Based on the concept of heat transfer enhancement elaborated above, the porous media are considered to be a kind of satisfying inserts for enhancing heat transfer in the tube flow, for its excellent performance in temperature uniformity. Lots of investigations have proven that partially filling a duct or channel with porous media is an effective method for heat transfer enhancement. Al-Nimr and co-workers [4] investigated numerically the transient forced convection of laminar flow in the developing region of parallel-plate ducts filled partially with porous inserts, and studied the effects of several operating parameters including porous layer thickness, Darcy number, thermal conductivity ratio, and microscopic inertial coefficient on the flow hydrodynamics and thermal characteristics. Kuznetsov [5] studied the similar problem of the fully developed forced convection in a parallel-plate channel with a porous medium in the center by means of mathematical analysis, and the analytical solutions for the critical parameters of heat transfer were obtained. Furthermore, he presented a more comprehensive

* Corresponding author. Tel.: +86 27 87542618.
E-mail address: w_liu@hust.edu.cn (W. Liu).

0017-9310/$ - see front matter © 2009 Elsevier Ltd. All rights reserved.
doi:10.1016/j.ijheatmasstransfer.2009.10.038

Nomenclature

A	cross-section area of the tube
C_p	specific heat of air at constant pressure
C_F	inertia coefficient
D	diameter
f	friction factor
h	convective heat transfer coefficient
I	electric current
K	permeability
L	length of the test section
Nu	Nusselt number
p	pressure
PEC	performance evaluation criteria
Pr	Prandtl number
q	heat flux
Q	heat gained by air
Q_e	exterior heat input
Q_v	volume flow rate of air
r	radial position measured from centerline
R	radius
Re	Reynolds number
R_{rad}	porous radius ratio
S	distance between two adjacent screens
T	temperature
u	axial velocity
u_m	average velocity of air
U_d	Darcian velocity
U_i	axial velocity of the air at the inlet of the test section
$\vec{U}$	velocity vector
v	radial velocity
V	voltage
z	axial position measured from the beginning of the test section

Greek symbols

α	local synergy angle, degree
δ	thickness of the annular channel
ε	porosity
μ	viscosity
θ	dimensionless temperature
λ	thermal conductivity
ρ	density

Subscripts

a	air
eff	effective
i	inner diameter or inlet value
m	mean value
o	outer diameter or outlet value
p	solid matrix of porous
s	smooth tube
w	wall

analytical investigation on this problem, considering different porous medium positions, flow directions and heating modes in Ref. [6]. New boundary layer type analytical solutions were obtained for these fundamentally important partly porous configurations. Alkam and Al-Nimr [7] introduced another method by inserting porous substrates at both sides of the inner tube wall, the thermal performance of a conventional concentric tube heat exchanger can be improved. The improvement was investigated numerically and the results showed that inserting the porous substrate may enhance the effectiveness of the heat exchanger considerably, although it increases the pressure drop within the heat exchanger at the same time. Kuznetsov [8] numerically studied the heat transfer of turbulent flow in a composite porous/fluid duct with porous media attached to the duct wall by using a two-layer k–ε model to account for interface roughness. The results showed that the roughness of the porous/fluid interface significantly impacts turbulent flow in the clear fluid region as well as overall heat transfer in the duct, and an unexpected feature that there is a minimum of dependence of the Nu number on the position of the interface was found and explained. Experimental works in this area were also performed. Hetsroni et al. [9] experimentally investigated the heat transfer and pressure drop in a rectangular channel with low porosity sintered porous inserts. The results showed that the heat sink has good performance of heat transfer, when it also leads to a drastic increase in the pumping power. Angirasa [10] experimentally studied the effectiveness of metallic fibrous with high porosity (above 90%) in heat transfer enhancement by mounting a fibrous heat block in a wind tunnel with air flow, demonstrated that the metallic porous heat dissipaters can achieve substantial heat transfer augmentation when compared to plain flat plate.

Actually, many scholars have studied heat transfer enhancement methods which are directed at the core region of a tube, but no one had developed the concept of enhanced heat transfer in the core flow. Mohamad [11] numerically investigated the problem of heat transfer enhancement for a laminar flow in a pipe fully or partially filled with porous medium inserted at the core of the conduit. It was shown that with the porous material partially filling in the core of a conduit, the rate of heat transfer from the wall can be increased with a reasonable pressure drop, and the thermally developing length can be reduced by 50% or more. This partially filling method works better than the fully filled one. Yang and Hwang [12] numerically investigated the turbulent fluid flow behavior and heat transfer enhancements in a pipe fully or partially filled with porous medium inserted at the core of the conduit. The impact of Re number, Da number and porous radius ratio on heat transfer performance was analyzed in detail. Chen and Sutton [13] numerically proposed and solved a developing duct flow with a porous insert in the center. The effect of both convection and radiation were taken into account and the radiative transfer is simulated by a special integral equations developed by themselves [14,15] with high accuracy. The results showed that the porous insert enhance both convective and radiative transfer. Pavel and Mohamad [16] further investigated the enhanced heat transfer effect of metallic porous materials that are inserted into the core of a pipe with a constant and uniform heat flux experimentally and numerically. The results obtained showed that compared with the clear flow case where no porous materials was used, higher heat transfer rates can be achieved using porous inserts whose diameters approach the diameter of the pipe and it is very important to get the accurate physical parameters of a porous material from the experiment for a successful numerical simulation. Wang et al. [17] experimentally and numerically investigated heat transfer enhancement by inserting metallic filament in a square channel without contact with the channel wall. The results indicated that the temperature profiles of fluid flowing over the filament become more uniform and the fluid temperature drops more sharply near the channel wall so that heat transfer was enhanced. Bharadwaj et al. [18] experimentally investigated the thermal performance of water flow in a 75-start spirally grooved tube with twisted tape insert. It is found that compared to smooth tube, the heat transfer enhancement due to spiral grooves is further augmented by inserting

twisted tapes, and the direction of twist (clockwise and anticlockwise) also influences the thermo-hydraulic characteristics.

Based on the concept of enhanced heat transfer in the core flow, the present study investigates the heat transfer enhancement and the flow resistance of air flow through a tube with porous medium inserts emplaced in the core of it under the constant uniform heat flux condition. The porous insert is developed to directly improve the uniformity of temperature profile in the tube and consequently to enhance convective heat transfer. Both numerical and experimental studies are performed to examine the effect of the porous insert on heat transfer for laminar to fully developed turbulent tube flow. The present work differs from previous work of Pavel and Mohamad [16] in few aspects: (a) characteristics of the turbulent flow are measured for the first time; (b) the performance evaluation criteria (*PEC*) is used to evaluate the integrated effect of the porous inserts on heat transfer enhancement intuitively; (c) the porous media used experimentally are different from theirs in terms of porosity, permeability, material used as well as porous radius ratio.

2. Problem definition

The problem is schematically presented in Fig. 1, in which the air, with a uniform inlet velocity and temperature, flows through a tube partially filled with porous media, and is heated by the tube wall with a constant and uniform heat flux. Both experimental and numerical study investigate the heat transfer enhancement over a range of Reynolds numbers about 1000–19,000 covering laminar, transitional, and the turbulent regime (for convenience, the transitional flow and turbulent flow are collectively referred to as turbulent flow in the following statement), and the heat flux is determined to make the temperature of the air rise about 10 °C after it flows through the tube. The porous media used for experiments are developed by cutting the commercial copper screen (8978 kg/m^3 in density and 387.6 W/(m^2 K) in thermal conductivity) to many circular pieces with a same diameter, inserting them on a thin copper rod evenly from the center then soldering to fix them together. The screens have 10 meshes in one inch and the wire diameter is 0.49 mm, meaning that the size of the meshes is 2 mm×2 mm. The internal diameter of the stainless steel tube D_i for experiments is 17 mm and its external diameter D_o is 19 mm. To partially fill the tube with porous media, the copper screens are cut out at a diameter D_p of 16 mm; that is, the thickness of the channel δ between the porous media and the wall is 0.5 mm and the porous radius ratio R_{rad} ($R_{rad} = R_P/R_i$; R_P is radius occupied by porous media while R_i is the internal radius of the tube) is about 0.94. Three different porous medium inserts are made by varying the distance S between two adjacent screens, which are 5 mm, 10 mm and 20 mm, respectively. The porosity ε of each porous medium is calculated by the volume ratio of the porous insert to all the screens on it. There are $\varepsilon = 0.951$, 0.966 and 0.975 correspond to the three different porous media inserts of $S = 5$, 10 and 20 mm, respectively.

3. Experimental apparatus and procedure

Experiments are conducted in a rig with air as the working fluid. Its schematic diagram is depicted in Fig. 2. The rig is composed of several stainless steel tube sections which joint together by flanges. Air is continuously supplied by a three-lobe Roots Blower (2) with discharge pressure of 44.1 kPa and flow capacity of 1.35 m^3/min. In order to minimize vibrations and flow pulsations, a 500 mm long stainless steel hose (4) and a tank (5) of about 0.2 m^3 in volume with two layers of semi-circular plate inside are successively connected with the air blower. The volume flow rate Q_v through the test section is measured by the vortex precession flow meter (8) which has ±1% accuracy and it is protected by the 90 μ-filter (7).The flow rate of air flowing inside the rig is regulated by two ways: (a) change the rev of the blower by transducer (1) which controls the AC frequency of the electric power required by the blower; (b) regulate the valve (6) in the bypass section. A rectifier (9) composed of two screens 100 mm apart from each other is installed at the entrance of the calming section (10) to remove eddies and provide a more uniform velocity profile. The calming section is 1.5 m long for the air flow can be hydrodynamic fully developed. The 300 mm length test section (12) follows the calming section. Two pressure taps are welded in the proximity of the exit and entrance flanges of the test section so that pressure drop through the test section can be measured by connecting them to the ports of the differential pressure transmitter (11) which has ±1% accuracy. The test section is heated at the exterior over its entire length with a uniform heat flux, which is generated by winding heater wire on the tube without any spacing between successive turns. The heater wire is covered with porcelain sleeves of 2 mm OD for insulation. The heating power can be regulated by the voltage regulator (14) connected to the heater wire. Then a voltage stabilizer (15) is connected between the local power network and the voltage regulator to remove the voltage fluctuation of the local power network when experiments proceed. To prevent heat loss from the environment, two layers of insulation materials are put on the test section. Firstly, the insulated heater wire is covered by an 80 mm thick asbestos tightly. Then dozens of sponge stripes are wound around the asbestos layer and the total thickness of the insulation materials is about 130 mm. The axial conduction loss from the connecting flanges is prevented by using double-decked PTFE spacers. Temperatures of the air entering and leaving the test section and those of the surface of the test section tube wall are measured by 10 K-type thermocouples which are all calibrated with an uncertainty of about ±0.5% in the operating temperature range. Five of them are soldered on the

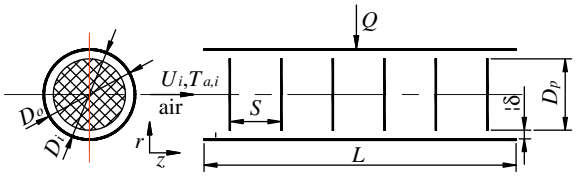

Fig. 1. Schematic diagram of the problem.

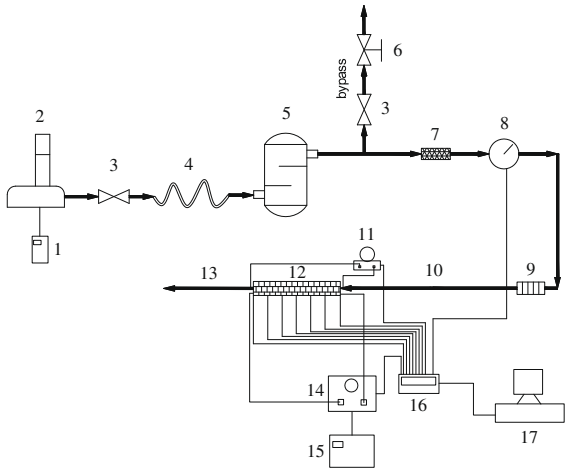

1. Transducer 2. Roots blower 3. Valve 4. Stainless steel hose 5. Tank 6. Regulatory valve 7. Filter 8. Gas flow meter 9. Rectifier 10. Calming section 11. Differential pressure transmitter 12.Test section 13.exit section 14. Voltage regulator 15. Voltage stabilizer 16. Signal conditioning unit 17. Computer

Fig. 2. Experimental rig layout.

tube wall with equal interval along the length of the test section and four are placed at flow cross-section at the exit of the test section with different radial positions of 0, 3, 6 and 8 mm, respectively to measure the temperature of the heated air accurately. All the electrical signals generated by the sensors are transmitted to the signal conditioning unit (16) and the resulting signals are further converted into digital signals by a DAQ card installed into a PC (17) so that the values including current, voltage, temperatures, pressure drop and flow rate can be recorded with an application associated with the signal conditioning unit. The whole acquisition system has an uncertainty of ±0.05%.

The experiments were carried out at different flow rates of air under constant wall heat flux conditions. The power input changes with the variation of the flow rate to make the temperature of the air rise by about 10 °C after it flows through the test section. The experimental procedures are as follows. Air with an initial flow rate was supplied to the experiment rig by the blower and a relevant power input was also supplied to the test section. The volume flow rate of air, the current and voltage of the power input, the temperature of the outside tube wall and the air at the inlet and outlet of the test section as well as the pressure drop were continuously monitored with a scanning frequency of 0.1 Hz. Generally it took approximately 7–8 h to reach steady-state condition for laminar flow of the initial experiment, and 4–5 h for turbulent flow. The steady-state condition here means that the temperatures indicated by the thermocouples do not vary by more than ±0.2 °C within a period of about 30 min. To effectively remove the noise specific to each sensor as well as the noise induced in the electric wires by the surrounding electromagnetic fields, each data point was obtained by averaging 200 discrete values acquired in almost 30 min. After collecting a set of data at steady-state condition of the initial flow rate, the frequency of the transducer was increased so that the air flow rate was changed to next value. It usually took a period of approximately 1.5 h to reach the steady-state again and then a new set of data was collected.

4. Data processing

As mentioned above, the volume flow rate of air Q_v, the current of the power input I, the voltage of the power input V, the average temperature of the outside tube wall $T_{w,o,m}$ (evaluated by taking arithmetic average of the five temperatures measured by the thermocouples soldered on the tube wall), the bulk temperatures of the air at the inlet $T_{a,i}$ and outlet $T_{a,o}$ of the test section, as well as the pressure drop Δp can be gained from a set of experiment data. Then the average velocity u_m of the air can be evaluated from $u_m = Q_v/A$, and the nominal cross-sectional area $A = \pi D_i^2/4$. The Reynolds number is defined based on nominal diameter as

$$Re = \rho u_m D_i/\mu, \tag{1}$$

and the friction factor is defined as

$$f = \frac{\Delta p}{L}\frac{2D_i}{\rho u_m^2}, \tag{2}$$

where L is the length of the test section. The sensible heat gained by air can be evaluated using relation

$$Q = Q_v \rho (T_{a,o} - T_{a,i}) C_p, \tag{3}$$

and the heat balance can be checked by comparing Q with the exterior heat input to air Q_e which is defined as $Q_e = IV$. The heat balance errors of all the experiment results were limited to less than 5%. Then the average convective heat transfer coefficient of the test section is evaluated as

$$h = \frac{Q}{\pi D_i L}\frac{1}{L}\int_0^L \frac{dz}{(T_{w,i} - T_{a,m})}, \tag{4}$$

where $T_{a,m}$ is the average air temperature in the test section, here $T_{a,m} = (T_{a,o} - T_{a,i})/2$, and $T_{w,i}$ is the inside tube wall temperatures. It can be evaluated from the outside tube wall temperatures in this case using one-dimensional heat conduction equation

$$T_{w,i} = T_{w,o} - \frac{Q \cdot \ln(D_o/D_i)}{2\pi\lambda_w L}, \tag{5}$$

where $T_{w,o}$ is the temperatures measured by thermocouples soldered on the tube wall and λ_w is thermal conductivity of stainless steel evaluated at $T_{w,o,m}$. The averaged Nusselt number is then evaluated as

$$Nu = hD_i/\lambda_a. \tag{6}$$

All the physical properties of air are evaluated at $T_{a,m}$ by linear interpolation and the International System of Units is used for all the physical values.

According to the uncertainties of measurement above (see Section 3), the uncertainty in the data calculation is analyzed based on Ref. [19]. The uncertainties in determining the physical parameters of the air and physical dimensions of the tube are estimated as 0.2% and 1.0%, respectively. Therefore, the maximum uncertainties of non-dimensional parameters are ±5.93% for Nusselt number, ±10.96% for friction factor and ±2.75% for Reynolds number. Furthermore, to verify the accuracy of experimental data, heat transfer experiments of smooth tube were done and the results of average Nusselt number and friction factor were compared to the results of corresponding traditional empirical relations (see Fig. 3). The accuracy of the experimental data is satisfactory for the relative errors are less than 3% compared to the results of empirical relations. The following equations are used as the empirical relations for verification. For friction factor of laminar flow ($1000 < Re < 2300$), it is

$$f_s = 64/Re, \tag{7}$$

and for friction factor of turbulent flow ($3000 < Re < 20{,}000$), the Blasius equation is

$$f_s = 0.3164/Re^{0.25}. \tag{8}$$

For verification of Nusselt number, the Gnielinski equation is used for turbulent flow

$$Nu_s = 0.0214(Re^{0.8} - 100)\mathrm{Pr}^{0.4} \cdot [1 + (D_i/L)^{2/3}](T_{a,m}/T_{w,i,m})^{0.45}, \tag{9}$$

and for laminar flow, no empirical relation can apply to the experiment situation in the test section, where velocity profile of the air is fully developed but temperature profile under the constant wall heat flux condition hasn't been developed yet, so a numerical simulation of heat transfer with the same condition in this case were done and the results are used to verify the Nusselt number of the experiments in laminar flow condition. The accuracy of the numerical model is checked by calculating the Nusselt number of a fully developed laminar flow under the constant wall heat flux condition and the results exactly equal to 4.364, which is the theoretical value in this condition. The results of the numerical simulation are correlated as

$$Nu_s = 0.84562Re^{0.29137}, \tag{10}$$

and the maximal fitting error is 0.6%.

As we know that in the numerical simulation, two physical properties of the porous media have to be determined, they are permeability K and inertia coefficient C_F. In order to make the numerical predictions more accurate, these two properties were experimentally determined by using the Darcian equation with Forcheimer revision

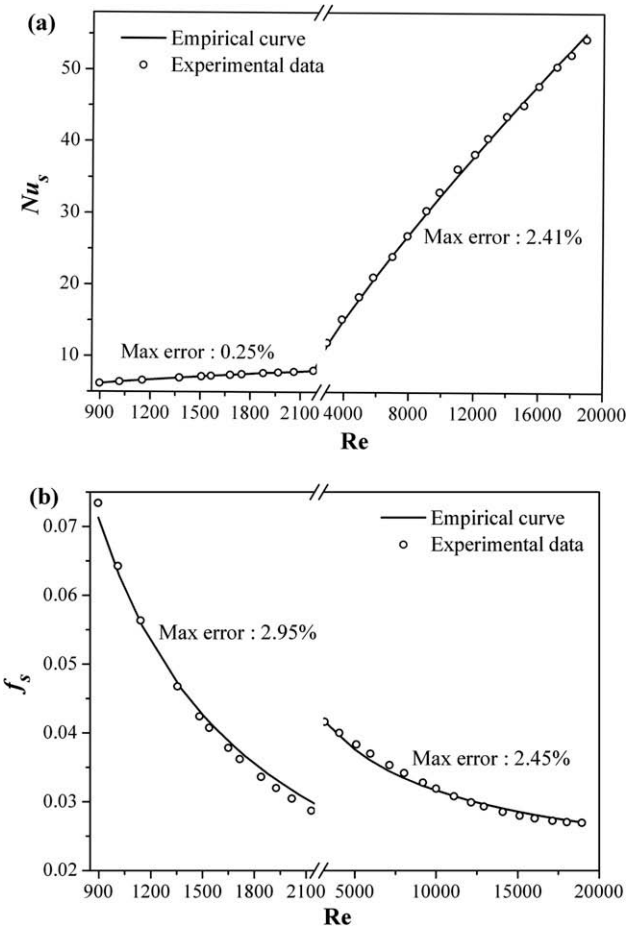

Fig. 3. Comparison of experimental results with the corresponding values of empirical relations for clear flow: (a) Nusselt number; (b) friction factor.

$$\Delta p = \frac{\mu L}{K} U_d + \frac{\rho L C_F}{\sqrt{K}} U_d^2, \tag{11}$$

where U_d is the Darcian velocity. It is easy to find that the pressure drop Δp is a quadratic function of the Darcian velocity U_d. It means that pressure drops over the porous inserts in a tube with the same diameter of the porous media at different Darcian velocities should be measured and the permeability K and inertia coefficient C_F can be calculated by fitting second order polynomials of Δp versus U_d through the experimental data. The pressure drops measured at different flow velocities over the porous media are presented in Fig. 4. The solid lines in the figure are the fitting curves of the experimental data. The corresponding values of permeability K (1.964×10^{-7} m^2, 3.064×10^{-7} m^2 and 5.721×10^{-7} m^2) and inertia coefficient C_F (0.017, 0.016 and 0.015) have been calculated for the three different porous media inserts of $\varepsilon = 0.951$, 0.966 and 0.975, respectively.

5. Mathematic model of numerical simulation

The problem of numerical simulation has been described previously (see Fig. 1). The air with uniform inlet velocity and temperature flows through a tube partially filled with porous media, and is heated by the tube wall at a constant and uniform heat flux. In the numerical simulation, the flow is considered to be two-dimensional with symmetry about the centerline. In order to develop the mathematic model, following assumptions are made: (a) the porous media are homogeneous and isotropic with no distension or contraction; (b) the analysis domain is subjected to local thermal equilibrium; (c) the heat generated by the viscous effects is negligible; (d) the gravitational effect of the air flowing through the tube is negligible; (e) steady-state flow is considered.

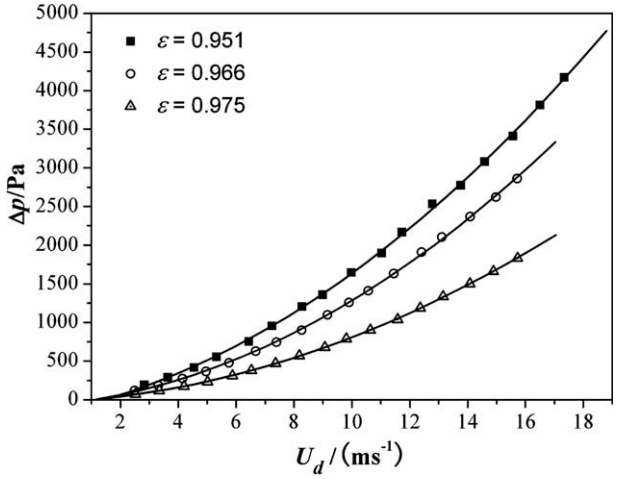

Fig. 4. Pressure drops measured at different flow velocities.

Continuity equation:

$$\frac{\partial}{\partial z}(\rho u) + \frac{1}{r}\frac{\partial}{\partial r}(r\rho v) = 0 \tag{12}$$

Momentum equations in porous region:

$$\frac{1}{\varepsilon^2}\frac{\partial}{\partial z}(\rho u u) + \frac{1}{r\varepsilon^2}\frac{\partial}{\partial r}(r\rho v u) = -\frac{\partial p}{\partial z} - \frac{\mu u}{K} - \frac{\rho F}{\sqrt{K}}\sqrt{u^2+v^2}\,u + \frac{1}{\varepsilon}\frac{\partial}{\partial z}\left(\mu\frac{\partial u}{\partial z}\right) + \frac{1}{r\varepsilon}\frac{\partial}{\partial r}\left(r\mu\frac{\partial u}{\partial r}\right) \tag{13a}$$

$$\frac{1}{\varepsilon^2}\frac{\partial}{\partial z}(\rho u v) + \frac{1}{r\varepsilon^2}\frac{\partial}{\partial r}(r\rho v v) = -\frac{\partial p}{\partial r} - \frac{\mu v}{K} - \frac{\rho F}{\sqrt{K}}\sqrt{u^2+v^2}\,v + \frac{1}{\varepsilon}\frac{\partial}{\partial z}\left(\mu\frac{\partial v}{\partial z}\right) + \frac{1}{r\varepsilon}\frac{\partial}{\partial r}\left(r\mu\frac{\partial v}{\partial r}\right) - \frac{\mu}{\varepsilon}\frac{v}{r^2} \tag{13b}$$

Momentum equations in non-porous region:

$$\frac{\partial}{\partial z}(\rho u u) + \frac{1}{r}\frac{\partial}{\partial r}(r\rho u v) = -\frac{\partial p}{\partial z} + \frac{\partial}{\partial z}\left(\mu\frac{\partial u}{\partial z}\right) + \frac{1}{r}\frac{\partial}{\partial r}\left(r\mu\frac{\partial u}{\partial r}\right) \tag{14a}$$

$$\frac{\partial}{\partial z}(\rho u v) + \frac{1}{r}\frac{\partial}{\partial r}(r\rho v v) = -\frac{\partial p}{\partial r} + \frac{\partial}{\partial z}\left(\mu\frac{\partial v}{\partial z}\right) + \frac{1}{r}\frac{\partial}{\partial r}\left(r\mu\frac{\partial v}{\partial r}\right) - \mu\frac{v}{r^2} \tag{14b}$$

Energy equation in porous region:

$$\frac{\partial}{\partial z}(\rho u C_p T) + \frac{1}{r}\frac{\partial}{\partial r}(r\rho v C_p T) = \frac{\partial}{\partial z}\left(\lambda_{eff}\frac{\partial T}{\partial z}\right) + \frac{1}{r}\frac{\partial}{\partial r}\left(r\lambda_{eff}\frac{\partial T}{\partial r}\right) \tag{15}$$

where λ_{eff} is the effective thermal conductivity of the medium defined by

$$\lambda_{eff} = (1-\varepsilon)\lambda_p + \varepsilon\,\lambda_a. \tag{16}$$

Energy equation in non-porous region:

$$\frac{\partial}{\partial z}(\rho u C_p T) + \frac{1}{r}\frac{\partial}{\partial r}(r\rho v C_p T) = \frac{\partial}{\partial z}\left(\lambda_a\frac{\partial T}{\partial z}\right) + \frac{1}{r}\frac{\partial}{\partial r}\left(r\lambda_a\frac{\partial T}{\partial r}\right) \tag{17}$$

Boundary conditions:

$$z = 0: \quad u = U_i, \quad v = 0, \quad T = T_{a,i} \tag{18a}$$

$$z = L: \quad \frac{\partial u}{\partial z} = 0, \quad v = 0, \frac{\partial T}{\partial z} = 0 \tag{18b}$$

$$r = 0: \quad \frac{\partial u}{\partial r} = 0, \quad v = 0, \frac{\partial T}{\partial r} = 0 \tag{18c}$$

$$r = R_i: \quad u = 0, \quad v = 0, \quad \lambda_a \frac{\partial T}{\partial r} = q \tag{18d}$$

The partial differential Eqs. (12)–(18) are solved by the control volume, finite difference approach and the SIMPLER algorithm is used for pressure-velocity coupling. The discretization of the momentum and energy equations employs the second order upwind format. The k–ε model of double equations is used for turbulent flow cases. In turbulent flow simulation, following assumptions are made: (a) steady-state condition is considered; (b) the variation of the air thermal properties is neglected for the relative small temperature range encountered; (c) there is no energy transfer by conduction in the tube wall. The spatial mesh points are set as 2300×52 in the computational domain. The criteria for convergence are to conserve mass, momentum and energy globally and locally. As one of the convergence criteria, relative variations of velocity and temperature between two iterations are set to be smaller than 10^{-8}. For a typical computation, 5000–6000 iteration steps are required to meet the accuracy. The meshes in boundary layer region are refined for accurate simulation. In order to check the grid independence of the results, meshes in different sizes of 1150×27, 2300×52 and 4600×90 in axial and radial directions, respectively, were employed in the grid test, where $\varepsilon = 0.951$, $R_{rad} = 0.94$, and $Re = 1000$ for laminar flow and 10,000 for turbulent flow were used. Average temperature of the heating tube wall and pressure drop of the test section were selected as the parameters for error analysis in the grid test. According to the test results, the mesh size of 2300×52 was used for all computations because the differences of the two error parameters were less than 0.0004% and 0.0295% respectively for laminar flow, and 0.0053% and 0.1400% for turbulent flow, compared to the case with mesh size of 4600×90. Moreover, the mesh size of 2300×52 has been validated by calculating the Nusselt number of a fully developed laminar flow under the constant wall heat flux condition and the results exactly equaled to 4.364, which has been mentioned in Section 4.

After finding out velocity and temperature fields, heat transfer coefficient of tube flow can be calculated as

$$h(z) = \frac{q}{T_{w,i}(z) - T_{a,m}(z)}, \tag{19}$$

where $T_{a,m}(z)$ is the cross-sectional bulk temperature of air inside the tube, and is evaluated by

$$T_{a,m}(z) = \int_0^{R_i} uTrdr \Big/ \int_0^{R_i} urdr. \tag{20}$$

Then the Nusselt number and friction factor can be calculated as

$$Nu(z) = h(z)D_i/\lambda_a, \tag{21}$$

$$f(z) = 2\frac{dp}{dz}D_i \Big/ \rho u_m(z)^2 \tag{22}$$

where $u_m(z)$ is the cross-sectional average velocity defined as

$$u_m(z) = 4\int_0^{R_i} 2\pi urdr \Big/ \pi D_i^2. \tag{23}$$

6. Experimental results and discussions

The results of average Nusselt number calculated from the experimental data are presented in Fig. 5. It can be seen that the average Nusselt number of all three porous medium inserts increases with the rise of Re in both laminar and turbulent flow overall. The values in turbulent flow regime are apparently larger than the ones in laminar flow regime, with the maximum reached approximately up to 120 obtained at about Re = 19,000. The variation in porosity ε has a strong influence upon the Nusselt number. Smaller ε leads to higher Nu value, which is the very characteristic of porous medium heat transfer. It is because a smaller ε makes the cross-sectional area available for fluid flow smaller and thus results in a higher flow velocity for heat transfer enhancement. In the experiment condition, smaller ε also means that more air tends to flow through the annular channel between the porous medium and the tube wall, which leads to a higher velocity in the vicinity of the tube wall and enhances the heat transfer significantly. From Fig. 5 it can also be seen that the Nusselt number for $\varepsilon = 0.966$ is closer to the one for $\varepsilon = 0.975$ than $\varepsilon = 0.951$ in laminar flow, which is considered to be the result of the smaller difference in ε value. But this is not the case for turbulent flow, where the Nusselt number for $\varepsilon = 0.966$ is closer to the one for $\varepsilon = 0.951$, especially in large Reynolds numbers. It suggests that for different Reynolds numbers, the heat and momentum interactions are complex, and for turbulent flow, a further increase in ε value has greater negative influence on the heat transfer performance than for laminar flow when ε is relatively large. Fig. 6 displays the variation of friction factor for different Reynolds numbers and porosities. As the characteristic of a flow in a rough tube, the friction factor decreases with the increase of Re in the whole range of velocity experimentally tested, and the trends tend to gentle as the Re increases. When

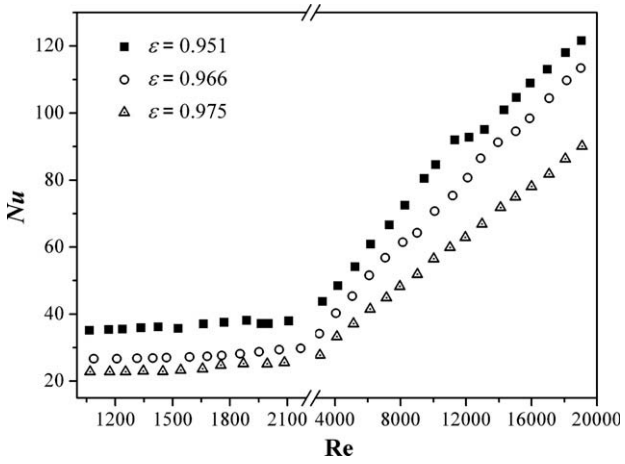

Fig. 5. Experimental results of Nusselt number.

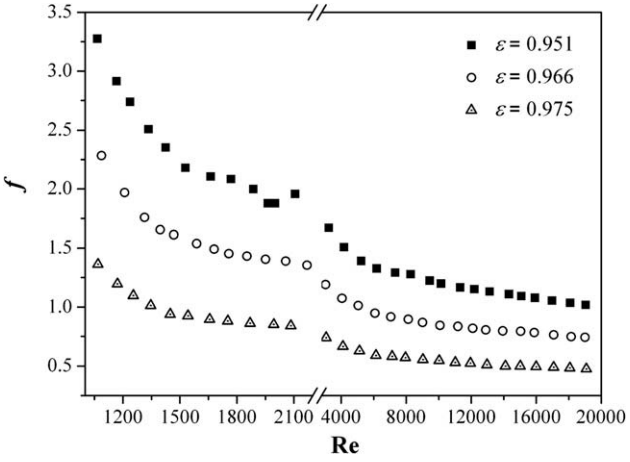

Fig. 6. Experimental results of friction factor.

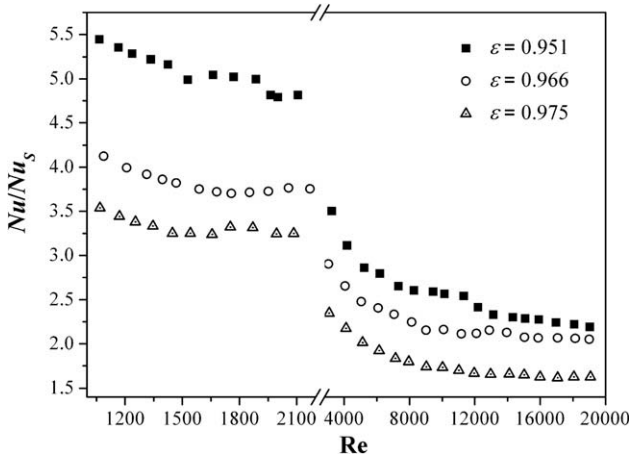

Fig. 7. Increase of heat transfer compared with smooth tube.

Re > 10,000, the friction factor is going to be constant for the same porosity. For the same *Re* value, the friction factor decreases when the porosity increases, which is expected because the smaller the porosity, the larger the pressure drop over the porous medium insert. It can also be seen that the impact on the friction factor of the porosity is less noticeable in the turbulent flow than in the laminar flow. Generally speaking, adopting porous medium insert with higher porosity is positive for lowering pressure drop of fluid, but negative for improving heat transfer rate between fluid and tube wall, which can be clearly observed in Figs. 5 and 6.

The comparison of thermal and hydrodynamic performance between the tube with porous medium inserts and the smooth tube is made by calculating the ratios of Nu/Nu_s and f/f_s. The results are presented in Figs. 7 and 8, respectively. In Fig. 7, it can be seen that inserting porous medium in the core of tube can heighten the heat transfer rate greatly compared to a smooth tube. The largest increase in the Nusselt number is higher than 5 times achieved by $\varepsilon = 0.951$ in the laminar flow. However, the heat transfer augmentation in turbulent flow regime is much worse than the laminar flow, and the change of the ratio of Nu/Nu_s with Reynolds number is not obvious in part of the turbulent flow range when *Re* > 15,000. This is because the relatively high flow velocity and a more uniform temperature of the turbulent flow, which weaken the enhanced effect for heat transfer of inserting porous medium in the core of tube. Fig. 8 shows the ratios of f/f_s in both laminar flow and turbulent flow. It is seen that great increase in flow resistance is gained by the use of porous medium inserts and it is more terrible in laminar flow than in turbulent flow. The ratio remains nearly constant along with *Re* in turbulent flow while there is a minimum at about *Re* = 1400 in laminar flow. Additionally, the impact of the porosity on the friction factor increase, arise from the use of porous inserts, is much less for turbulent flow than laminar flow.

In order to assess the heat transfer enhancement under constant pumping power, the following formula of performance evaluation criteria is employed [20]

$$PEC = \frac{Nu/Nu_s}{(f/f_s)^{1/3}}. \tag{24}$$

Fig. 9 displays the variation of *PEC* value at different Reynolds numbers and porosities. In laminar flow, the *PEC* values for all the porosity are larger than 1, which means that the augmentation of heat transfer can cover the penalty arising from the increased flow resistance and this is a sign of good performance in heat transfer, but it is not the case in turbulent flow where nearly all the *PEC* values are less than 1. It suggests that although heat transfer rate is increased by the application of porous media, the flow resistance increases even more in turbulent flow, which weaken the integrated performance. The *PEC* values decreases with the increase in *Re* while it is more complicated for the relation between *PEC* and the porosity ε, which corresponds to the distance *S* between two adjacent screens. The best performance is obtained when $\varepsilon = 0.951$ in almost the whole range of *Re* experimentally tested except *Re* > 13,000. It is worth noting that in the laminar flow, *PEC* values for $\varepsilon = 0.975$ are somewhat higher than those for $\varepsilon = 0.966$, which means that the *PEC* values do not have linear change with ε (or *S*) in laminar flow. There may be an optimal ε (or *S*) value for enhancing heat transfer in the laminar flow. In the turbulent range of *Re*, however, *PEC* values for $\varepsilon = 0.966$ exceed those for $\varepsilon = 0.975$ and even being the highest when *Re* > 15,000. It is considered that flow and temperature fields in the tube have very complex interactions and there are many factors influencing the integrated performance of enhanced heat transfer.

It can be found from the analysis of the experimental results that, for turbulent flow, the impact of porosity on every performance parameters used above is less than that for laminar flow. As we know, the porosity ε is an important parameter of porous media and a crucial factor to the media's ability of dissipation and uniformity, then in turbulent flow, as the flow velocity is higher and the temperature is more uniform than those in laminar flow, the dissipation and uniformity effect from using porous inserts is weakened; consequently, the impact of the porosity on heat transfer performance is diminished.

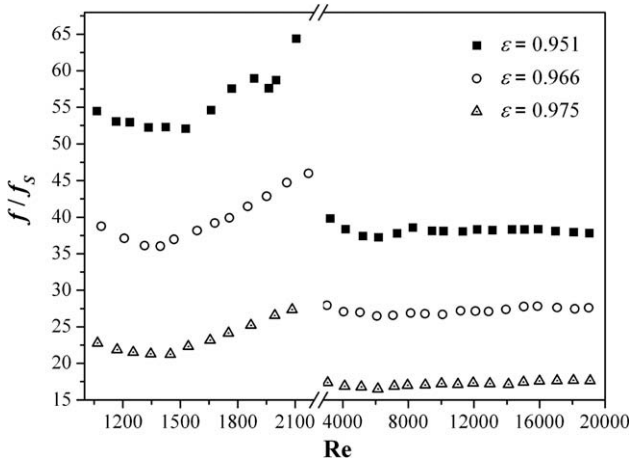

Fig. 8. Increase of friction factor compared with smooth tube.

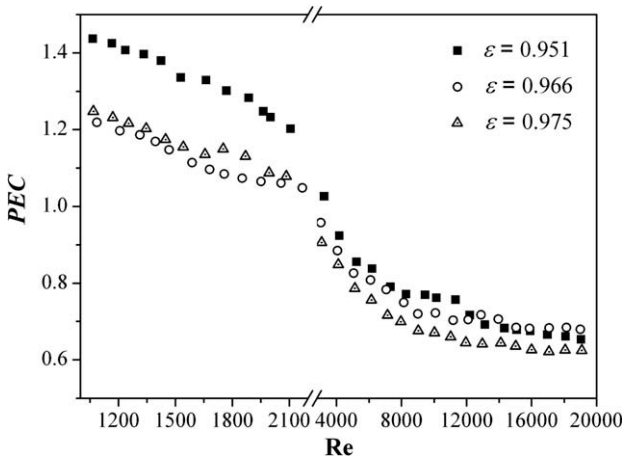

Fig. 9. *PEC* values versus Reynolds number.

7. Numerical results and discussions

In order to verify the correctness of the concept of enhanced heat transfer in the core flow, thermal and hydrodynamic performance for different porous radius ratios R_{rad} are investigated numerically to make up deficiencies in experiments. The permeability K and inertia coefficient C_F of the porous media in numerical investigation are determined by experimental data (see Section 4) as described earlier. Furthermore, the principle of field synergy (presented by Guo et al. [21]) is applied to analyze the synergy between temperature profiles and velocity profiles in the fluid flow. At last, numerical simulation with the same condition of the experiments is done for comparison.

7.1. Influence of R_{rad}

Fig. 10 presents the dimensionless temperature difference and velocity profiles of the fluid at the middle cross-section of the test section for different R_{rad} values compared to clear flow cases, which is impossible to be obtained from experiments. The dimensionless temperature difference here is defined as

$$\theta = (T_{w,i} - T_a)/(T_{w,i} - T_{a,m}). \quad (25)$$

It is readily seen in Fig. 10(a) that the employment of a porous medium made the temperature distribution uniform at the core of tube (namely the region with porous media), it is because that the thermal conductivity of the porous solid matrix is much larger than the air and therefore the effective thermal conductivity at the core of tube is modified greatly. Moreover, because of the uniform temperature in the core flow, a great dimensionless temperature gradient compared to the case of clear flow is formed in the vicinity of the tube wall, which will lead to a high heat transfer rate. It is also seen that the increase in porous ratio R_{rad} enlarges the core flow region with uniform temperature, and consequently raises the temperature gradient near the wall. When R_{rad} value is up to 0.94, the temperature profile is constant in most part of the cross-section and makes the thermal boundary layer very thin. It is expected that the method of enhanced heat transfer in the core flow will work better in a fully developed flow cases where no thermal boundary layer exists, because an equivalent thermal boundary layer could be formed in this way to gain better thermal performance.

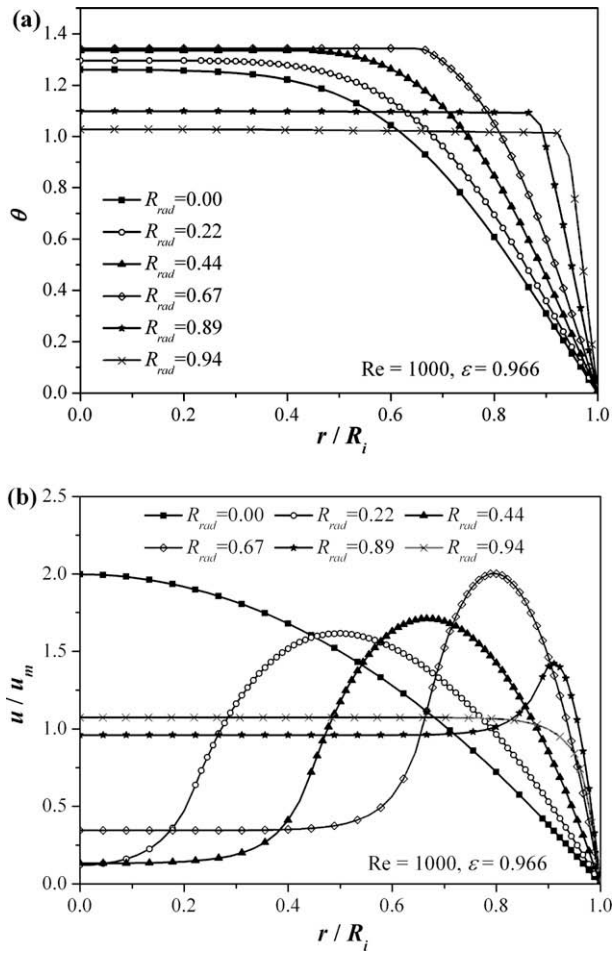

Fig. 10. Dimensionless profiles at the middle cross-section for different radius ratio of: (a) temperature; (b) velocity.

The dimensionless velocity profiles are shown in Fig. 10(b). As expected, because of the decrease in the cross-section area, partially filling the tube with porous medium increases the velocity gradient near tube wall compared to clear flow case, which will increase not only the heat transfer rate but also the flow resistance. It can also be seen that due to Darcian resistance from the solid matrix of porous media, more air flows through the annular channel between porous matrix and the tube wall, which leads to a peak of velocity at the core of the channel. The maximum velocity of the fluid increases and shifts toward the tube wall with the increase in R_{rad} up to 0.67, after which the peak values decrease and the velocity profiles turn to uniform. When R_{rad} = 0.94, the peak of velocity even disappears, which is positive for decreasing growth rate of the flow resistance. It is considered to be resulted from the increase in flow resistance of the annular channel with the increase in R_{rad} (namely the decrease in size of the annular channel). The ratio of flow resistance between the annular channel and porous region apparently influences the velocity profile of the flow.

Fig. 11 displays the influence of R_{rad} on heat transfer performance for Re = 1000 and ε = 0.966. Both Nusselt number and friction factor ratios increase along with R_{rad} and the gradients become larger and larger, except the case in friction factor that R_{rad} value changes from 0.89 to 0.94 where the growth rate keeps the same trend with the anterior case. This may be due to the disappearance of the velocity peak located near the tube wall (see Fig. 10(b)). In Fig. 11(b) it is easy to find that the *PEC* values decline as the R_{rad} increases until R_{rad} reaches 0.67, then begins to increase after that and furthermore a sharp increase appears when R_{rad} = 0.94. In this case, the augmentation of heat transfer is greater than the increase in friction factor. It means that the effect of temperature uniformity on integrated performance of heat transfer becomes more and more obvious along with the R_{rad} increase when R_{rad} > 0.67, and a good *PEC* value of approximately 1.27 is obtained when R_{rad} = 0.94. However, the value of R_{rad} should be less than 1 to avoid a great increase in flow resistance, which is demonstrated by Mohamad [11]. All this can be summed up into two conclusions: (a) it is the improvement of the uniformity of temperature profile, instead of the change of velocity field, that plays a major role in heat transfer enhancement, it is the basis of the core flow enhancement; (b) when using porous inserts for enhancing heat transfer, the value of R_{rad} should be large enough (but less than 1 of course) and this value relates to the physical properties of the porous medium including porosity ε and permeability K, which impact on the Darcian resistance of the porous. So the value of R_{rad} and ε should be chosen moderately for use in enhancing heat transfer.

7.2. Field synergy analysis

According to the principle of field synergy, the convection term in the energy Eqs. (17) and (19) can be corresponded to the heat source term in the conduction equation. Heat transfer can be enhanced through a source enhancement. It is reflected in the

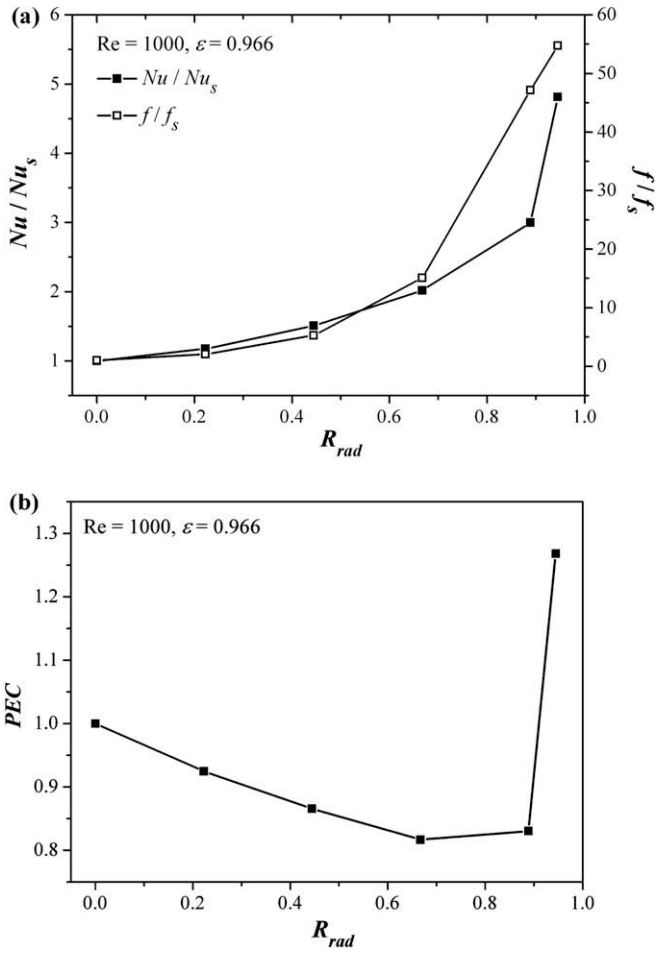

Fig. 11. Influence of R_{rad} on heat transfer performance: (a) ratios of *Nu* and *f* with smooth tube; (b) *PEC* values.

synergy between velocity field and temperature field of fluid, namely the synergy angle α between fluid-velocity vector and temperature gradient vector in the flow field, which is expressed as

$$\cos\alpha = \frac{\vec{U}\cdot\nabla T}{|\vec{U}|\cdot|\nabla T|}. \tag{26}$$

Reducing synergy angle α can enhance heat transfer. Fig. 12 displays the local synergy angle distributions at the middle cross-section of the test section for different R_{rad} compared with the smooth tube, it is seen that the local synergy angle in the region with porous material decreases notably, by which heat transfer is enhanced largely. Further increase in the R_{rad} enlarges the region with small synergy angle and the average synergy angle in the whole domain will be reduced, so the *Nu* number will consequently increase at the same time. This evince that unlike the traditional boundary enhancement, the core enhancement is an effective way for enhancing heat transfer.

The variation of average synergy angle of the test section with *Re* number when R_{rad} = 0.94 and ε = 0.951 is shown in Fig. 13. As expected, the average synergy angles in turbulent flow regime of a ranging from 25° to 65° approximately are obviously larger than the ones in laminar regime. The change of the angles along with *Re* is nonlinear for turbulent flow, while the gradient gets smaller as *Re* increases. The comparison of the average synergy angle between laminar and turbulent flow once again illustrates that the integrated heat transfer performance of this type of porous inserts

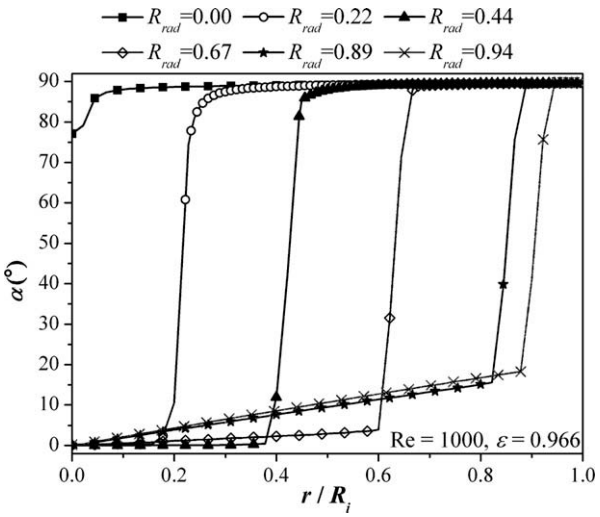

Fig. 12. Variation of local synergy angle with radius ratio.

in turbulent flow regime is dissatisfactory and far way from the case for laminar flow.

7.3. Comparison

The comparison of Nusselt number and friction factor between experimental results and numerical predictions is presented in Table 1. It can be found that both experimental and numerical results show the similar tendency for *Nu* and *f*, and most numerical results agree well with the measured data, which is manifested by the fact that error of 75% of the *Nu*-data is less than 20% and error of 87% of the *f*-data is less than 10%. The error is considered to be reasoned by three factors: (a) the porous model used in numerical simulation is homogeneous and isotropic, where heat conduction exists when fluid flows. While the porous inserts tested in experiments are homogeneous but anisotropic as they were manufactured by inserting different numbers of screens on metallic rods, heat conduction in which is very weak. This will lead to the numerical results larger than the experimental ones for *Nu* number. Furthermore, the area contact with the fluid for experimental porous inserts is smaller than the numerical continuous porous model because of their non-continuous structures, which will result in the numerical results over predict the values of *f* for experiments; (b) comparing to the numerical cases, the non-continuous structure

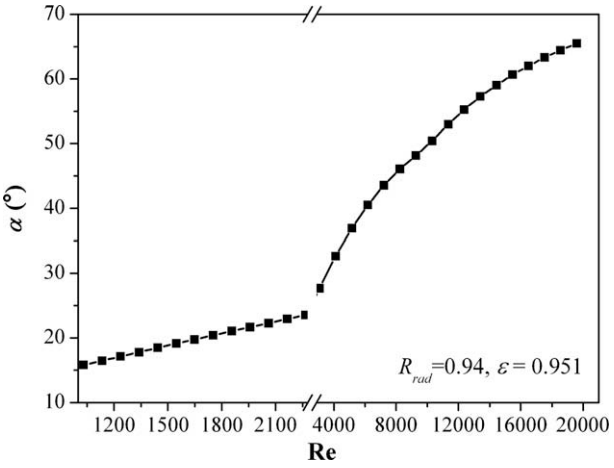

Fig. 13. Variation of average synergy angle with *Re* when R_{rad} = 0.94 and ε = 0.951.

Table 1
Comparison between numerical predictions and experimental results.

ε	*Re*	*Nu* (exp.)	*Nu* (num.)	Error (%)	*f* (exp.)	*f* (num.)	Error (%)	*Re*	*Nu* (exp.)	*Nu* (num.)	Error (%)	*f* (exp.)	*f* (num.)	Error (%)
0.951	1064	35.11	30.11	14.26	3.27	3.03	7.40	5234	54.13	42.21	22.03	1.39	1.42	2.39
	1165	35.41	30.79	13.07	2.91	2.85	2.35	6184	60.93	46.62	23.48	1.32	1.31	1.31
	1237	35.56	31.20	12.26	2.73	2.73	0.39	7318	66.59	52.54	21.11	1.29	1.21	5.93
	1334	35.90	31.68	11.77	2.50	2.59	3.46	8276	72.51	57.94	20.10	1.27	1.16	9.37
	1424	36.17	32.06	11.39	2.35	2.48	5.65	9444	80.46	64.86	19.39	1.22	1.11	9.13
	1529	35.73	32.44	9.23	2.17	2.37	8.85	10,152	84.61	69.19	18.23	1.19	1.09	9.07
	1661	37.02	32.83	11.33	2.10	2.25	7.01	11,317	91.94	76.43	16.87	1.16	1.06	8.92
	1768	37.58	33.11	11.92	2.08	2.17	4.06	12,198	92.71	81.97	11.60	1.15	1.04	9.34
	1887	38.10	33.38	12.41	1.99	2.08	4.25	13,124	95.06	87.83	7.61	1.12	1.03	9.19
	1963	37.19	33.53	9.84	1.87	2.04	8.41	14,336	100.98	95.53	5.40	1.10	1.00	9.67
	2001	37.17	33.61	9.61	1.87	2.01	7.16	15,082	104.64	100.31	4.14	1.09	0.98	9.96
	2106	37.95	33.80	10.95	1.95	1.95	0.13	15,928	108.90	105.79	2.87	1.07	0.97	10.44
	2219	38.79	33.98	12.41	1.90	1.90	0.53	16,977	113.05	112.70	0.32	1.05	0.95	10.19
	3238	43.79	35.20	19.63	1.67	1.80	7.85	18,087	117.95	120.25	1.94	1.03	0.93	9.75
	4172	48.48	38.04	21.55	1.50	1.60	5.88	19,049	121.54	127.10	4.57	1.01	0.92	8.34
0.966	1086	26.74	31.06	16.16	2.28	2.10	8.00	5059	45.37	37.33	17.72	1.01	1.01	0.06
	1207	26.68	31.63	18.55	1.97	1.96	0.49	6075	51.57	40.32	21.81	0.95	0.94	1.22
	1314	26.85	32.04	19.30	1.76	1.85	5.32	7060	56.82	43.97	22.61	0.92	0.88	3.59
	1395	26.93	32.30	19.95	1.65	1.78	7.89	8142	61.46	48.61	20.91	0.90	0.84	5.84
	1467	27.04	32.50	20.19	1.61	1.73	7.23	9019	64.26	52.70	17.98	0.87	0.82	5.72
	1587	27.17	32.79	20.67	1.54	1.65	7.15	10,089	70.80	57.96	18.13	0.84	0.80	5.29
	1679	27.42	32.97	20.24	1.49	1.59	6.79	11,174	75.39	63.44	15.85	0.83	0.78	6.50
	1756	27.66	33.12	19.71	1.45	1.55	6.86	12,098	80.68	68.16	15.52	0.82	0.77	5.93
	1851	28.18	33.28	18.10	1.43	1.51	5.22	12,895	86.53	72.23	16.53	0.81	0.76	5.47
	1950	28.71	33.43	16.44	1.41	1.46	4.15	13,955	91.30	77.63	14.97	0.80	0.75	6.15
	2057	29.45	33.57	13.99	1.39	1.42	2.25	15,051	94.55	83.21	11.99	0.79	0.73	7.58
	2170	29.82	33.71	13.07	1.36	1.38	1.89	15,880	98.46	87.44	11.19	0.78	0.72	7.81
	2267	30.22	33.82	11.91	1.33	1.35	1.48	17,065	104.47	93.61	10.40	0.76	0.71	7.26
	3033	34.13	34.74	1.79	1.19	1.25	4.91	18,140	109.77	99.44	9.40	0.75	0.70	6.22
	4052	40.24	35.39	12.05	1.07	1.11	3.81	19,001	113.49	104.40	8.01	0.74	0.70	5.74
0.975	1068	22.83	31.24	36.86	1.36	1.28	5.95	5126	37.20	36.05	3.10	0.63	0.66	4.79
	1171	22.82	31.63	38.62	1.20	1.21	1.28	6144	41.55	38.20	8.08	0.59	0.61	3.22
	1254	22.85	31.89	39.56	1.10	1.16	5.66	7134	44.96	40.85	9.15	0.58	0.58	0.93
	1346	23.00	32.14	39.72	1.01	1.11	9.77	7962	48.28	43.38	10.15	0.57	0.55	2.56
	1448	22.93	32.36	41.11	0.94	1.06	13.32	9023	51.90	46.92	9.60	0.55	0.54	3.38
	1542	23.36	32.54	39.32	0.93	1.03	10.81	10,035	56.52	50.50	10.66	0.54	0.52	4.17
	1656	23.75	32.72	37.76	0.90	0.99	10.27	11,025	59.93	54.10	9.74	0.53	0.51	3.25
	1752	24.80	32.86	32.46	0.88	0.96	8.54	11,959	62.88	57.53	8.52	0.52	0.50	3.76
	1869	25.22	33.00	30.84	0.86	0.93	7.11	12,971	66.85	61.24	8.40	0.51	0.50	2.92
	1994	25.17	33.14	31.68	0.85	0.89	4.97	14,116	71.85	65.39	8.98	0.50	0.49	2.41
	2085	25.51	33.23	30.23	0.84	0.87	4.08	15,024	75.05	68.66	8.51	0.50	0.48	4.10
	2156	25.92	33.29	28.43	0.82	0.86	4.88	15,995	78.10	72.15	7.61	0.49	0.47	4.92
	2214	26.22	33.34	27.17	0.82	0.85	3.76	17,073	81.82	76.07	7.03	0.49	0.46	5.25
	3075	27.76	34.26	23.42	0.74	0.81	10.23	18,076	86.34	79.82	7.55	0.48	0.46	5.20
	4112	33.26	34.67	4.25	0.67	0.72	8.63	19,078	90.13	83.77	7.06	0.48	0.46	3.99

of experimental porous inserts also increases flow disturbance, especially in large range of *Re*. This will enhance not only heat transfer but also flow resistance, so the experimental results are going to be larger than the numerical ones both for *Nu* and *f* values motivated by this reason; (c) contact of some screens with the tube wall may exist in the test section, so conductive heat transfer may take place between the tube wall and the porous inserts in experiments, but it is not the case in numerical simulation. Based on this point it is reasonable to expect the numerical results under predict the values of *Nu* obtained experimentally, but it has only a little impact on friction factor.

The errors between experimental results and numerical simulations result from the combined effect of the three factors above. It can be found in Table 1 that the numerical results of *Nu* are from smaller to larger than the experimental results in laminar flow range of *Re* and increases along with porosity ε. A larger ε means a larger distance *S* between two adjacent screens and its degree of anisotropic and non-continuous is deepen, so the effect of factor (a) will be more obvious than the factor (b) and (c). This inference can also be proved by the fact that experimental results of *Nu* is larger than numerical ones in turbulent range of *Re* for all cases of ε, since a large *Re* number is going to make up for the deficiency of weak heat conduction in the experimental porous matrix. This means the experimental porous inserts are more similar to the numerical porous models in large *Re*. In addition, factor (b) is more active when *Re* increase, thus the numerical results of *Nu* are under predicted compared to the experimental ones in large range of *Re*. On the other hand, the regularities of errors in friction factor *f* are similar for different porosities (see Table 1). The experimental results are smaller than the numerical ones for the laminar flow since the effect of factor (a) prevails over factor (b) in this range of *Re* and, due to the effect of factor (b) comes more and more strong as *Re* number increases, the opposite regularity is observed in turbulent flow.

8. Conclusions

(1) Inserting a porous medium at the core of tube is experimentally proved to be an effective way for heat transfer enhancement. The heat transfer rate of the tube with porous inserts whose diameters approach the diameter of the tube is about 1.6–5.5 times larger than the smooth tube cases in laminar, transitional and turbulent ranges of Reynolds numbers. However, the flow resistance increases at the same time. The experimental results of *PEC* indicates that the method has good integrated performance of heat transfer enhancement

in laminar flow where the *PEC* values are larger than 1 with the maximum value of about 1.44 obtained in $Re = 1000$ and $\varepsilon = 0.951$.

(2) The measurements indicate that flow and heat transfer in the tube with porous medium inserts are influenced by complex interactions between momentum and heat transfer in the fluid flow, resulting in non-monotonic behavior of *PEC* values with porosity ε. It is that the *PEC* values progressively decrease for $\varepsilon = 0.951$, 0.975 and 0.966 in turn in laminar flow, while in turbulent flow the sequence is $\varepsilon = 0.951$, 0.966 and 0.975. Furthermore, the integrated performance is better for small Reynolds numbers than large ones.

(3) Good agreement lies between numerical and experimental results. The numerical results show that the application of porous inserts effectively makes the temperature profiles of fluid flow become more uniform at the core of tube, which play a major role in heat transfer enhancement. Moreover, the porous radius ratio R_{rad} should be large enough but less than 1 to obtain a good integrated performance by using porous inserts for enhancing heat transfer. As a result, heat transfer is enhanced greatly with an acceptable flow resistance increase. It shows that unlike the traditional boundary enhancement, the core flow enhancement is an efficacious method for enhancing heat transfer. This is also verified according to the principle of field synergy by the fact that average synergy angles of the fluid flow can be reduced notably by the usage of porous inserts compared to the clear flow cases.

(4) The employment of porous media leads to a great increase in heat transfer rate; however, due to the structural features of the porous media, its employment also enlarges the contact area between the porous media and the fluid flow at the same time, thus increases the flow resistance significantly. As a result, the effect of enhanced heat transfer is relatively poor for turbulent flow. Nonetheless, according to the concept of heat transfer enhancement in the core flow, it is possible to develop inserts for enhancing heat transfer in tube flow with better integrated performance in large flow rates.

Acknowledgement

This work was supported by the National Key Basic Research Development Program of China (No. 2007CB206903) and the National Natural Science Foundation of China (No. 50721005).

References

[1] R.M. Manglik, Heat transfer enhancement, in: A. Bejan, A. Kraus (Eds.), Heat Transfer Handbook, John Wiley & Son, Hobokin, New Jersey, 2003.
[2] R.L. Webb, Principles of Enhanced Heat Transfer, John Wiley, New York, 1994.
[3] W. Liu, K. Yang, A. Nakayama, Enhancing heat transfer in the core flow by forming an equivalent thermal boundary layer in the fully developed tube flow, in: Proceedings of the Sixth International Conference on Enhanced, Compact and Ultra-Compact Heat Exchangers, Potsdam, Germany, 2007.
[4] M.K. Alkam, M.A. Al-Nimr, M.O. Hamdan, Enhancing heat transfer in parallel-plate channels by using porous inserts, Int. J. Heat Mass Transfer 44 (2001) 931–938.
[5] A.V. Kuznetsov, Force convection heat transfer in a parallel-plate channel with a porous core, Int. J. Appl. Mechan. Eng. 4 (1999) 271–290.
[6] A.V. Kuznetsov, Analytical studies of forced convection in partly porous configurations, in: K. Vafai (Ed.), Handbook of Porous Media, Marcel Dekker, New York, 2000.
[7] M.K. Alkam, M.A. Al-Nimr, Improving the performance of double-pipe heat exchangers by using porous substrates, Int. J. Heat Mass Transfer 42 (1999) 3609–3618.
[8] A.V. Kuznetsov, Numerical modeling of turbulent flow in a composite porous/fluid duct utilizing a two-layer k–ε model to account for interface roughness, Int. J. Therm. Sci. 43 (2004) 1047–1056.
[9] G. Hetsroni, M. Gurevich, R. Rozenblit, Sintered porous medium heat sink for cooling of high-power mini-devices, Int. J. Heat Fluid Flow. 27 (2006) 259–266.
[10] D. Angirasa, Experimental investigation of forced convection heat transfer augmentation with metallic fibrous materials, Int. J. Heat Mass Transfer 45 (2002) 919–922.
[11] A.A. Mohamad, Heat transfer enhancements in heat exchangers fitted with porous media. Part I: constant wall temperature, Int. J. Therm. Sci. 42 (2003) 385–395.
[12] Y.T. Yang, M.L. Hwang, Numerical simulation of turbulent fluid flow and heat transfer characteristics in heat exchangers fitted with porous media, Int. J. Heat Mass Transfer 52 (2009) 2956–2965.
[13] X.L. Chen, W.H. Sutton, Enhancement of heat transfer: combined convection and radiation in the entrance region of circular ducts with porous inserts, Int. J. Heat Mass Transfer 48 (2005) 5460–5474.
[14] X.L. Chen, W.H. Sutton, Radiative transfer in finite cylindrical media using transformed integral equations, J. Quant. Spectrosc. Radiat. Transfer 77 (2003) 233–271.
[15] W.H. Sutton, X.L. Chen, A general integration method for radiative transfer in 3-D non-homogeneous cylindrical media with anisotropic scattering, J. Quant. Spectrosc. Radiat. Transfer 84 (2004) 65–103.
[16] B.I. Pavel, A.A. Mohamad, An experimental and numerical study on heat transfer enhancement for gas heat exchangers fitted with porous media, Int. J. Heat Mass Transfer 47 (2004) 4939–4952.
[17] S. Wang, Z.Y. Guo, Z.X. Li, Heat transfer enhancements by using metallic filament insert in channel flow, Int. J. Heat Mass Transfer 44 (2001) 1373–1378.
[18] P. Bharadwaj, A.D. Khondge, A.W. Date, Heat transfer and pressure drop in a spirally grooved tube with twisted tape insert, Int. J. Heat Mass Transfer 52 (2009) 1938–1944.
[19] ANSI/ASME, Measurement Uncertainty, PTC 19, 1-1985, 1986 Part I.
[20] W.Z. Gu, J.R. Shen, C.F. Ma, Y.M. Zhang, Heat Transfer Enhancement, Scientific Press, Beijing, 1990.
[21] Z.Y. Guo, W.Q. Tao, R.K. Shah, The field synergy (coordination) principle and its applications in enhancing single phase convective heat transfer, Int. J. Heat Mass Transfer 48 (2005) 180–1797.